Identification of feature genes and molecular mechanisms involved in cell communication in uveal melanoma through analysis of single-cell sequencing data

NING LYU[1-3*], JIAWEN WU[1-3*], YIQIN DAI[1-3*], YIDAN FAN[1-3], ZHAOYUAN LYU[4], JIAYU GU[1-3], JINGYI CHENG[1-3] and JIANJIANG XU[1-3]

[1]Eye Institute and Department of Ophthalmology, Eye & ENT Hospital, Fudan University, Shanghai 200031, P.R. China; [2]NHC Key Laboratory of Myopia and Related Eye Diseases, Key Laboratory of Myopia and Related Eye Diseases, Chinese Academy of Medical Sciences, Shanghai 200031, P.R. China; [3]Shanghai Key Laboratory of Visual Impairment and Restoration, Shanghai 200031, P.R. China; [4]Graduate School of Transdisciplinary Arts, Akita University, Akita 010-0195, Japan

Received February 8, 2024; Accepted July 5, 2024

DOI: 10.3892/ol.2024.14636

Abstract. Uveal melanoma (UM) is a highly metastatic cancer with resistance to immunotherapy. The present study aimed to identify novel feature genes and molecular mechanisms in UM through analysis of single-cell sequencing data. For this purpose, data were downloaded from The Cancer Genome Atlas and National Center for Biotechnology Information Gene Expression Omnibus public databases. The statistical analysis function of the CellPhoneDB software package was used to analyze the ligand-receptor relationships of the feature genes. The Metascape database was used to perform the functional annotation of notable gene sets. The randomForestSRC package and random survival forest algorithm were applied to screen feature genes. The CIBERSORT algorithm was used to analyze the RNA-sequencing data and infer the relative proportions of the 22 immune-infiltrating cell types. *In vitro*, small interfering RNAs were used to knockdown the expression of target genes in C918 cells. The migration capability and viability of these cells were then assessed by gap closure and Cell Counting Kit-8 assays. In total, 13 single-cell sample subtypes were clustered by t-distributed Stochastic Neighbor Embedding and annotated by the R package, SingleR, into 7 cell categories: Tissue stem cells, epithelial cells, fibroblasts, macrophages, natural killer cells, neurons and endothelial cells. The interactions in NK cells|Endothelial cells, Neurons|Endothelial cells, CD74_APP, and SPP1_PTGER4 were more significant than those in the other subsets. T-Box transcription factor 2, tropomyosin 4, plexin D1 (*PLXND1*), G protein subunit α I2 (*GNAI2*) and SEC14-like lipid binding 1 were identified as the feature genes in UM. These marker genes were found to be significantly enriched in pathways such as vasculature development, focal adhesion and cell adhesion molecule binding. Significant correlations were observed between key genes and immune cells as well as immune factors. Relationships were also observed between the expression levels of the key genes and multiple disease-related genes. Knockdown of *PLXND1* and *GNAI2* expression led to significantly lower viability and gap closure rates of C918 cells. Therefore, the results of the present study uncovered cell communication between endothelial cells and other cell types, identified innovative key genes and provided potential targets of gene therapy in UM.

Correspondence to: Professor Jianjiang Xu or Dr Jingyi Cheng, Eye Institute and Department of Ophthalmology, Eye & ENT Hospital, Fudan University, 83 Fenyang Road, Shanghai 200031, P.R. China
E-mail: jianjiangxu@126.com
E-mail: tippicjy@126.com

*Contributed equally

Key words: uveal melanoma, single-cell sequencing, cell communication, *PLXND1*, *GNAI2*

Introduction

Uveal melanoma (UM) is the most common primary intraocular malignancy in adults (1). UM typically arises from choroidal melanocytes (90%) and melanocytes in the ciliary body (6%) or iris (4%) (2). UM is a highly malignant and lethal tumor, with ~50% of patients dying within a decade of diagnosis owing to its high risk of metastasis (3,4). Patients with metastasis have a poor prognosis, and the treatment of metastatic UM remains challenging owing to a lack of understanding of the biological characteristics of this disease (5). To address this issue, metastasis doubling times have been calculated, and it has been hypothesized that primary UM cells start to spread several years before diagnosis and initial treatment (6). Genetic characteristics linked to UM include mutations in the G protein subunit α (*GNA*)*Q*, *GNA11* or eukaryotic translation initiation factor 1A X-linked genes (7). Alterations in gene expression associated with the occurrence of UM have also been demonstrated. For instance, loss of chromosome 3 and mutations in the BRCA1 associated protein 1 (*BAP1*) and

splicing factor 3b subunit 1 genes frequently increase the risk of metastasis, and *BAP1* is a tumor suppressor gene (8). In general, 1-2% of patients with UM carry germline alterations in the *BAP1* gene (9). UM tissue comprises not only tumor cells but also an array of diverse immune cells (10). There is a notable increase in the presence of a distinct type (M2-type macrophages) of immune cells in UM, which accelerate tumor growth through angiogenesis and immunosuppression as a significant role of immune responses in the process of UM metastasis (10,11).

One area of significance in cancer research is single-cell sequencing, an innovative technique that provides high-resolution insights into the cellular composition of tumor tissues, thus enabling the exploration of the rich landscape of cell-to-cell communication within the tumor microenvironment (12). Some UM studies based on single-cell sequencing have shown tumor heterogeneity and varying gene expression patterns. For instance, Pandiani *et al* (13) found that hes family bHLH transcription factor 6 was an effective target for inhibiting UM progression. In addition, Durante *et al* (14) reported that lymphocyte activating 3 was a potential candidate for immune checkpoint blockade in patients with high-risk UM. Cell communication plays an essential role in the progression of cellular malignancies, as the ability of invasive cells to communicate and influence their surroundings determines the metastatic potential and subsequent impact of the disease (15). However, the cell-cell communication nexus within UM remains largely unexplored. This research requires a concerted effort to unravel the complex connections among mRNAs, micro (mi)RNAs and long non-coding (lnc)RNAs in a cancer type that is rare yet impactful, and which affects the uvea of the eye.

At present, UM is typically treated with radiation therapy, laser therapy, local resection and enucleation, chemotherapy and immunotherapy; however, none of these methods have shown satisfactory results (16,17). Furthermore, while immunotherapy with checkpoint inhibition (such as anti-cytotoxic T-lymphocyte associated protein 4 and programmed cell death protein 1/programmed death-ligand 1 inhibitors) showed promising results in treating cutaneous melanoma, it did not appear to be as effective for UM (17,18). Thus, an improved insight into the molecular and genetic profiles of UM is essential to facilitate the detection of new prognostic biomarkers and to develop new treatment modalities specific for patients with UM.

The present study aimed to identify new feature genes involved in the occurrence of UM and provide deeper insights into the mechanism of UM, including subtype clusters, ligand-receptor interactions, immune infiltration, co-expressed UM genes and competing endogenous (ce)RNA networks, through analysis of single-cell sequencing data. *In vitro* assays were also performed to verify the biofunctions of the identified key genes.

Materials and methods

Data acquisition. A total of 80 samples with processed raw mRNA expression data from UM were downloaded from The Cancer Genome Atlas (TCGA) database (https://portal.gdc.cancer.gov/projects/TCGA-UVM) (19). TCGA database is currently the largest cancer genomics database and stores various types of cancer-related data, including gene expression, miRNA expression, copy number and DNA methylation data (20). The GSE138433 dataset was downloaded from the National Center for Biotechnology Information (NCBI) Gene Expression Omnibus (GEO; https://www.ncbi.nlm.nih.gov/geo/info/datasets.html) public database, which contained melanoma-related data for single-cell analysis (13). This dataset consisted of 6 samples. Briefly, the GEO database is a gene expression database created and maintained by the NCBI in the United States (21).

Single-cell analysis processing. First, the 'Seurat' package (v4; https://satijalab.org/seurat) (22) was employed to load the expression profile, followed by filtering out low-expressed genes using the criteria: nFeature_RNA >100 and percent.mt <5. Data were standardized, normalized and subjected to a principal component analysis (PCA). The ElbowPlot method identified the optimal number of principal components (PCs) as 13. Subsequently, data integration was performed among the samples using the 'harmony' package. Further analysis involved FindNeighbors, FindClusters and the t-distributed Stochastic Neighbor Embedding (t-SNE) method to visualize the spatial relationships between clusters with a specified resolution of 0.8.

The clusters were annotated using the 'celldex' (v1.0.0) and 'SingleR' packages (v1.4.1) (https://bioconductor.org/books/release/SingleRBook/sc-mode.html), revealing associations with crucial cells in disease occurrence. Finally, the FindAllMarkers function, with the logfc.threshold set to 1 and min.pct set to 0.25, was used to extract the marker genes for each cell subtype from the single-cell expression profile. Gene filtering criteria, including p_val_adj <0.01 and |avg_log2FoldChange|>1, was applied to identify significantly differentially expressed genes, serving as unique markers for each cell subtype.

Analysis of the interactions between ligands and receptors. CellPhoneDB (v4.0.0; https://github.com/ventolab/CellphoneDB) (23) is an openly available, curated repository of receptors, ligands and their interactions (24). Ligands and receptors consist of subunits that accurately represent heteromeric complexes. The ligand-receptor database, CellPhoneDB, is integrated with UniProt, Ensembl, PDB, IUPHAR and other resources. CellPhoneDB collectively stores 978 proteins, enabling a comprehensive and systematic analysis of communication molecules in cells and facilitating the study of intercellular communication and signaling networks in different cell types. A significance analysis of ligand-receptor relationships for features in the single-cell expression profiles was performed using the statistical_analysis function of the CellPhoneDB software package. The cluster labels of all cells were randomly permuted 1,000 times, and the average expression level of receptors within clusters and the average expression level of ligands within interacting clusters were determined. This generated a null distribution (also known as the Bernoulli distribution or binomial distribution) for each receptor-ligand pair in every pairwise comparison between two cell types. Finally, notable ligand-receptor pairs were selected for visualization.

Gene functional enrichment and protein-protein interaction (PPI) analyses. Functional annotation was performed on notable gene sets using the Metascape database (www.metascape.org) and the 'clusterProfiler' package (v3.18.1; https://bioconductor.org/packages/release/bioc/html/clusterProfiler.html) (25) to comprehensively explore the functional relevance of these gene sets. Gene Ontology (GO; https://metascape.org/gp/index.html) and Kyoto Encyclopedia of Genes and Genomes (KEGG; https://metascape.org/gp/index.html) analyses were performed for specific genes. A minimum overlap of ≥3 and P≤0.01 were considered to indicate statistical significance. PPIs were analyzed using Cytoscape software (3.9.1; https://cytoscape.org/) (26).

Random survival forest of selected key genes. Feature selection was performed using the 'randomForestSRC' package (v3.2.1; https://cran.r-project.org/web/packages/randomForestSRC/index.html) (27). Additionally, the random survival forest algorithm (v3.6.4) was used to rank the importance of prognosis-related genes (nrep=1,000, indicating 1,000 iterations in the Monte Carlo simulation). Genes with relative importance >0.5 were identified as the final marker genes.

Immune infiltration analysis. The CIBERSORT algorithm ('CIBERSORT' R package; v1.03; https://cibersortx.stanford.edu/) (28) was utilized to analyze RNA-sequencing data from different patient subgroups. This algorithm was used to infer the relative proportions of 22 immune-infiltrating cell types. A Pearson correlation analysis between gene expression levels and immune cell abundance was further performed. P<0.05 was considered to indicate a statistically significant difference.

Drug sensitivity analysis. Using the Genomics of Drug Sensitivity in Cancer (GDSC) database (https://www.cancerrxgene.org/), the R package 'pRRophetic (v0.5) was employed to predict the chemosensitivity of each tumor sample. Regression analysis was employed to obtain half-maximal inhibitory concentration estimates for specific chemotherapy drugs, and 10-fold cross-validation was performed using the GDSC training set to assess the accuracy of the regression and prediction. Default values were selected for all parameters, including using 'combat' to remove batch effects and averaging duplicate gene expression values.

Gene Set Enrichment Analysis (GSEA). GSEA of the expression profiles of patients with UM was performed using the GSEA tool (http://www.broadinstitute.org/gsea). This analysis was performed to identify the pathways enriched by differentially expressed genes between the high- and low-expression groups, distinguished by the median expression value of each key gene. Gene sets were filtered based on maximum and minimum gene set sizes of 500 and 15 genes, respectively. After 100 permutations, enriched gene sets were obtained based on P<0.05 and a false discovery rate of 0.25.

Construction of the nomogram and calibration curve. Overall survival (OS) curves were generated using the Kaplan-Meier (KM) method. Risk scores for each sample were calculated using the Cox proportional hazards model. Samples were divided into high-risk and low-risk groups based on the median risk score. A two-stage weighted test using the R package, 'TSHRC' (29), was then performed to validate the significance between the high-risk and low-risk groups.

Correlations between UM-related genes and feature genes. UM-related genes were obtained from the GeneCards database (https://www.genecards.org/) and then the expression levels of the top 20 genes with relevance score were compared with the expression levels of key genes. Analysis of the expression level of key genes and UM-related genes at the single cell level was also applied for comparison.

Construction of a lncRNA-miRNA-mRNA related ceRNA network. A potential lncRNA-miRNA-mRNA network was predicted using the miRWalk (http://mirwalk.umm.uni-heidelberg.de/) and ENCORI databases (https://rnasysu.com/encori/) and further validated using both the TargetScan (https://www.targetscan.org/vert_80/) and miRDB databases (https://mirdb.org/). Finally, ceRNA networks based on differentially expressed genes were constructed and visualized using Cytoscape software (version 3.9.1; https://cytoscape.org/) (26).

Cell culture and treatment. All experiments were performed in compliance with the Association for Research in Vision and Ophthalmology (https://www.arvo.org/About/policies/). The human UM C918 cell line (originated from choroid) was purchased from American Type Culture Collection (also termed MP41; cat. no. CRL-3297). C918 cells were cultured in fresh Dulbecco's Modified Eagle Medium/Nutrient Mixture F-12 (cat. no. 11320033; Thermo Fisher Scientific, Inc.) supplemented with 10% fetal bovine serum (cat. no. 10099141C; Thermo Fisher Scientific, Inc.) and 1% penicillin-streptomycin solution (cat. no. 15140122; Thermo Fisher Scientific, Inc.) at 37˚C and 5% CO_2 in a suitable incubator. For gene knockdown, small interfering (si)RNA duplexes targeting human genes [SEC14-like lipid binding 1 (*SEC14L1*), plexin D1 (*PLXND1*), tropomyosin 4 (*TPM4*) or *GNAI2*] and a control siRNA were designed and synthesized by Guangzhou RiboBio Co., Ltd. The C918 cells were seeded in 12-well plates at a density of $1x10^5$ cells/ml. When the cells reached a 50-60% confluency, the *SEC14L1*, *PLXND1*, *TPM4*, *GNAI2* or control siRNA (100 nmol/l) were transfected by riboFECT CP Transfection Kit (cat. no. C10511-05; Guangzhou RiboBio Co., Ltd.) according to the manufacturer's instructions. At 24 h post transfection, the cells were harvested and the knockdown efficiencies of *SEC14L1*, *PLXND1*, *TPM4* and *GNAI2* were evaluated using reverse transcription-quantitative polymerase chain reaction (RT-qPCR). The siRNA sequences of the target genes and the negative control are shown in Table I.

RNA extraction and RT-qPCR. Briefly, total RNA was extracted from different siRNA-treated C918 cells using TRIzol reagent (cat. no. 15596026; Thermo Fisher Scientific, Inc.). The RNA concentration was measured using a NanoDrop 2000 spectrophotometer (Thermo Fisher Scientific, Inc.). gDNA was erased at 42˚C for 3 min and the first-strand cDNA was reverse transcribed from 1 μg total RNA at 42˚C for 15 min followed by 95˚C for 3 min using the KR106 FastQuant RT Kit with gDNA Eraser (cat. no. KR106-03; Tiangen Biotech Co., Ltd.). Subsequently, qPCR was performed using a QuantiNova SYBR

Table I. Small interfering RNA sequences used in the present study.

Gene	Sequence, 5'-3'
GNAI2	Sense: GGACCUGAAUAAGCGCAAA
	Anti-sense: UUUGCGCUUAUUCAGGUCC
TPM4	Sense: UGCUGAAUUUGCAGAGAGA
	Anti-sense: UCUCUCUGCAAAUUCAGCA
SEC14L1	Sense: GCUGGAUUACAUCGACAAA
	Anti-sense: UUUGUCGAUGUAAUCCAGC
PLXND1	Sense: CCAUGAGUCUCAUAGACAA
	Anti-sense: UUGUCUAUGAGACUCAUGG
Negative control	Sense: UUCUCCGAACGUGUCACGU
	Anti-sense: ACGUGACACGUUCGGAGAA

GNAI2, G protein subunit α I2; TPM4, tropomyosin 4; SEC14L1, SEC14-like lipid binding 1; PLXND1, plexin D1.

Table II. Primer sequences used in reverse transcription-quantitative PCR.

Gene	Primer sequences, 5'-3'
GNAI2	Forward: CACCGCCGAGGAGCAAGG
	Reverse: CTCCAGGTCGTTCAGGTAGTAGG
TPM4	Forward: CCCTCAACCGACGCATCCAG
	Reverse: TCACCTTCATTCCTCTCTCA CTCTC
SEC14L1	Forward: GCTGGAGAACGAAGACC TGAAG
	Reverse: GACTGACGAGGCATCCACAATC
TBX2	Forward: GCTGACCAACAACATCTCTGA CAAG
	Reverse: AGGTGCGGAAGGTGCTGTAAG
PLXND1	Forward: GCCATCAAGCAGCAAATCA ACAAG
	Reverse: CCGCAGCAGCCACTCCTC
GAPDH	Forward: CGACCACTTTGTCAAGCTCA
	Reverse: AGGGGAGATTCAGTGTGGTG

GNAI2, G protein subunit α I2; TPM4, tropomyosin 4; SEC14L1, SEC14-like lipid binding 1; PLXND1, plexin D1; TBX2, T-Box transcription factor 2.

Green PCR kit (cat. no. 208054; Qiagen GmbH) according to the manufacturer's instructions. The qPCR primer sequences are shown in Table II. The housekeeping gene, GAPDH, was used per sample for normalization of the data using $2^{-\Delta\Delta Cq}$ (30).

Cell Counting Kit-8 (CCK-8) assay. C918 cells were treated as aforementioned then incubated with the CCK-8 reagent (cat. no. CK04-100T; Dojindo Laboratories, Inc.) at 37˚C for 2 h. The absorbance at 450 nm was measured using a spectrophotometer (Synergy H1 Hybrid Reader; BioTek; Agilent Technologies, Inc.). The cell viability of each group was calculated according to the manufacturer's instructions.

Gap closure assay. C918 cells were seeded at a density of $1x10^5$/ml cells on each side of the double-well culture inserts (cat. no. 80209; Ibidi GmbH) in a 24-well plate. After attachment, cells were respectively treated with control, *PLXND1* and *GNAI2* siRNA (100 nmol/l); 48 h post-transfection, the culture inserts were removed, and the cells were washed with PBS. The cells (in medium containing 1% FBS) were then allowed to migrate for a further 20 h. Cell migration was observed using an Olympus IX-73 microscope equipped with a color camera for light microscopy (Olympus Corporation). The gap closure rate of each group was evaluated by ImageJ software (v1.52a; National Institutes of Health).

Statistical analysis. All statistical analyses were performed using R language (https://cran.r-project.org/; v 4.1.3). Unpaired student's t-test was used for comparisons between two groups. For multiple comparisons, ANOVA followed by the Dunnett's test was applied. All data are presented as the mean ± SD. $P<0.05$ was considered to indicate a statistically significant difference.

Results

Single-cell sample subtype clustering and annotation analysis. A total of 19,441 cells with nFeature_RNA >100 and percent.mt <5 were included in the analysis (Fig. S1A and B). nfeatures=3,000 was set to merge batches of samples for subsequent analysis and to display the expression of genes in the samples (Fig. S1C). The top 10 genes with the highest standardized variance were then labeled (Fig. S1C). Through PCA (dimensionality reduction analysis) of the 10 genes, different scores were observed across different dimensions (Fig. S1D and E). However, when performing the PCA among samples, the overall differences were not significant (Fig. S1F). Based on ElbowPlot, the optimal number of PCs was determined to be 13 (Fig. S1G). Multi-sample integration of the single-cell samples using Seurat showed a small batch effect (Fig. 1A). A total of 13 subtypes were identified using t-SNE (Fig. 1B). Significant differences in the expression levels of numerous genes were observed among the subtypes. The dot plot visualization of the cell types were annotated manually to complement the results obtained from SingleR and showed that machine learning-based annotation significantly outperformed manual annotation in distinguishing various cell types (Fig. 1C). Using the R package SingleR to annotate each subtype, the 13 clusters were annotated into the following cell categories: 'Tissue_stem_cells', 'Epithelial_cells', 'Fibroblasts', 'Macrophage', 'NK_cell', 'Neurons' and 'Endothelial_cells' (Fig. 1D and E). Finally, using the FindAllMarkers function, 678 cell subtype marker genes were extracted from the single-cell expression profile (Table SI).

Analysis of receptor-ligand relationships and enriched pathways. Significant ligand-receptor pairs were selected for display, and the interactions in 'NK_cell|Endothelial_cells', 'Neurons|Endothelial_cells', 'CD74_APP' and 'SPP1_PTGER4' were the most significant (Fig. 2A). In addition, there

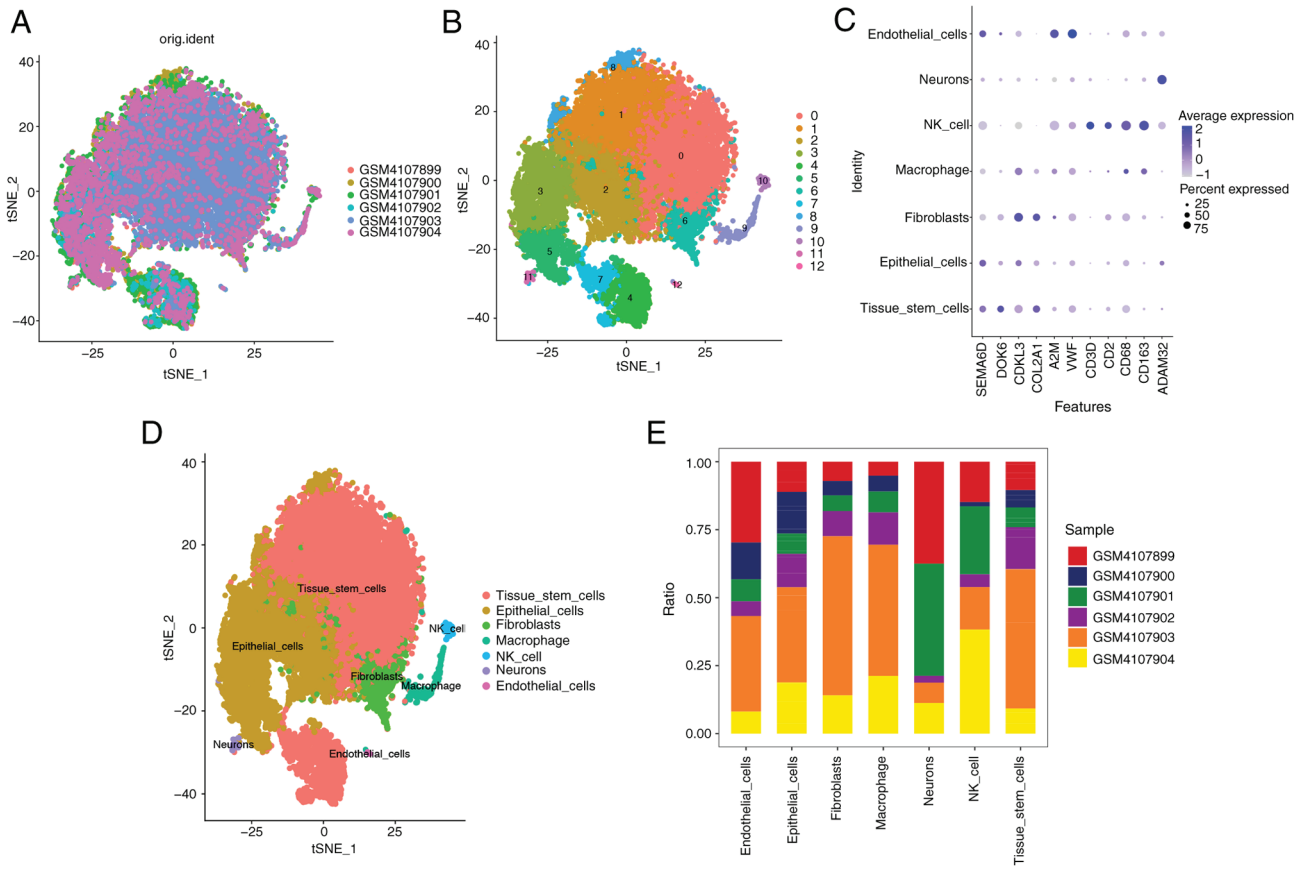

Figure 1. Single-cell sample subtype clustering analysis (GSE138433 dataset). (A) Multi-sample integration. (B) Subtypes identified by t-SNE. (C) The dot plot visualization of cell types. (D) Cell categories of clustered subtypes. (E) Proportion of samples in each category. NK, natural killer; t-SNE, t-distributed Stochastic Neighbor Embedding.

were large numbers of potential ligand-receptor pairs among 'Macrophages', 'NK_cell', 'Endothelial_cells' and other cell types (Fig. 2B). With respect to cell-cell communication, the cellular senescence pathway was positively correlated with 'Endothelial.cells-neurons' (P<0.01; Fig. 2C). As observed in the heatmap shown in Fig. S2, the neurons mainly originated from progenitor cells and cones, while endothelial cells had diverse sources including capillary, lymphatic, vascular and venous origins. The count of ligand-receptor gene pairs corresponding to each cell group indicated that the Endothelial_cells subtype had the highest number of interaction relationships among all cell subtypes (Fig. 2D). Using the Metascape database, pathway analysis of 299 marker genes from the Endothelial_cell subtype showed significant enrichment in several pathways. These included 'vasculature development', 'focal adhesion' and 'cell adhesion molecule binding' (Fig. 2E and F). Additionally, PPI network analysis of the genes within this marker gene set (Fig. 2G) showed that complex protein interactions existed in patients with UM.

Random survival forest analysis of key genes. To further identify the key genes in the marker gene set that influenced UM, a random survival forest analysis was conducted using the TCGA-UM cohort. Based on a relative importance of >0.5, 5 genes that met the selection threshold were identified as the final markers (Fig. 3A). Excepting T-Box transcription factor 2 (*TBX2*), the key genes had high expression levels in NK cells (Fig. 3B). Furthermore, neither NK cells nor macrophages showed high expression of *TBX2* (Fig. 3B). In the KM survival analysis, all 5 genes showed significant results in the TCGA-UM cohort, with the following order of significance: *TBX2*, *TPM4*, *PLXND1*, *GNAI2* and *SEC14L1*. Specifically, high expression levels of *TBX2*, *GNAI2*, *TPM4*, *PLXND1* and *SEC14L1* were associated with a longer OS time in UM (all P<0.05; Fig. 3C-G).

Immune microenvironment analysis of key genes. The tumor immune microenvironment is typically composed of tumor-associated fibroblasts, immune cells, extracellular matrix, various growth factors, inflammatory factors and specific physical and chemical characteristics, as well as cancer cells themselves (31). The immune microenvironment significantly affects the diagnosis, survival outcome and clinical treatment sensitivity of tumors. The relative percentage of different immune cell types in each sample was shown in Fig. 4A. There were multiple significant correlations among these immune cells, indicating complex biological interactions among inflammatory cells (Fig. 4B). *PLXND1* expression was most significantly positively correlated with monocytes and negatively correlated with plasma cells (both P<0.01; Fig. 4C). *TPM4* expression was most significantly positively correlated with follicular helper T cells and negatively correlated with M2 macrophages (both P<0.01; Fig. 4C). *GNAI2* expression was most significantly positively correlated with monocytes

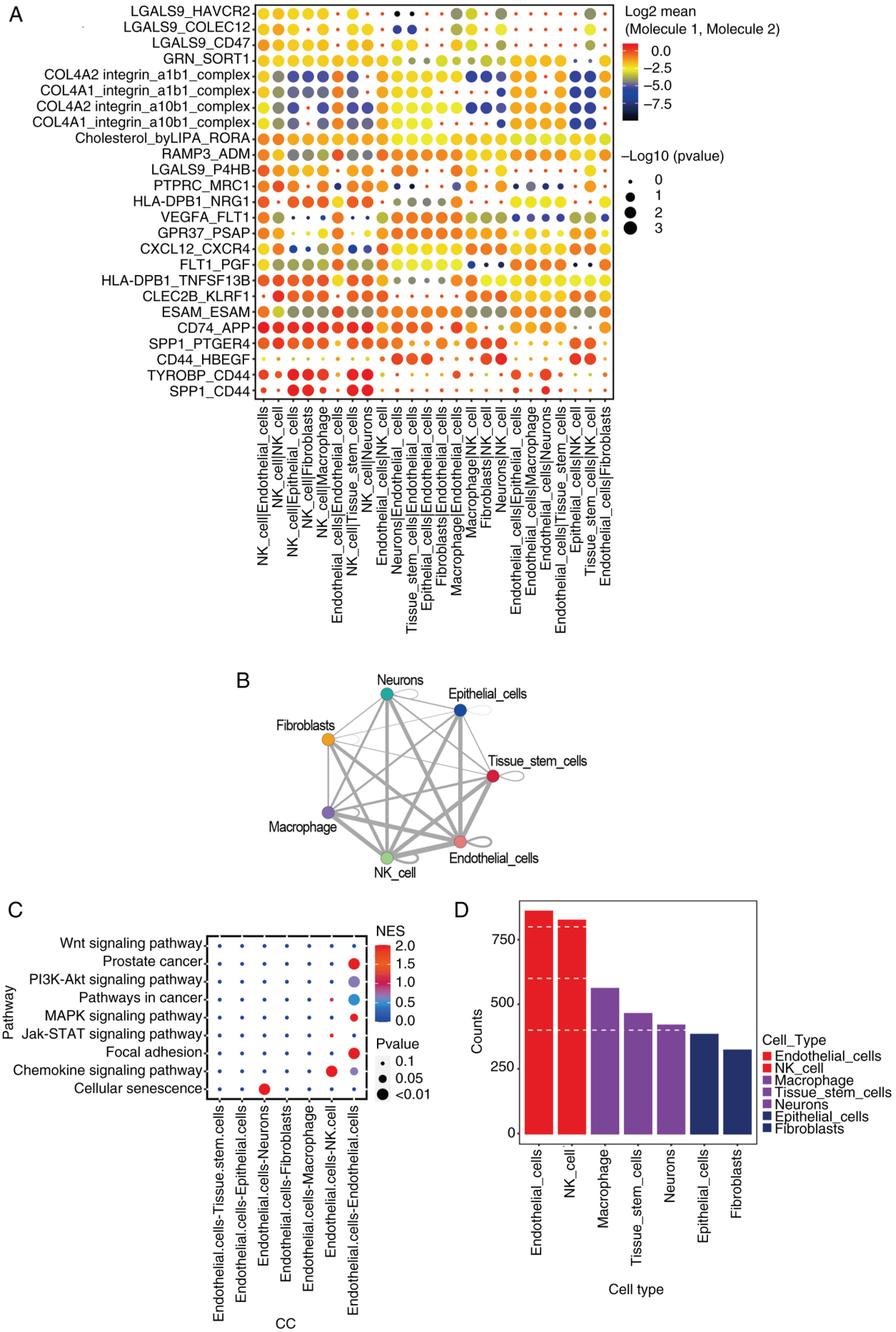

Figure 2. Continued.

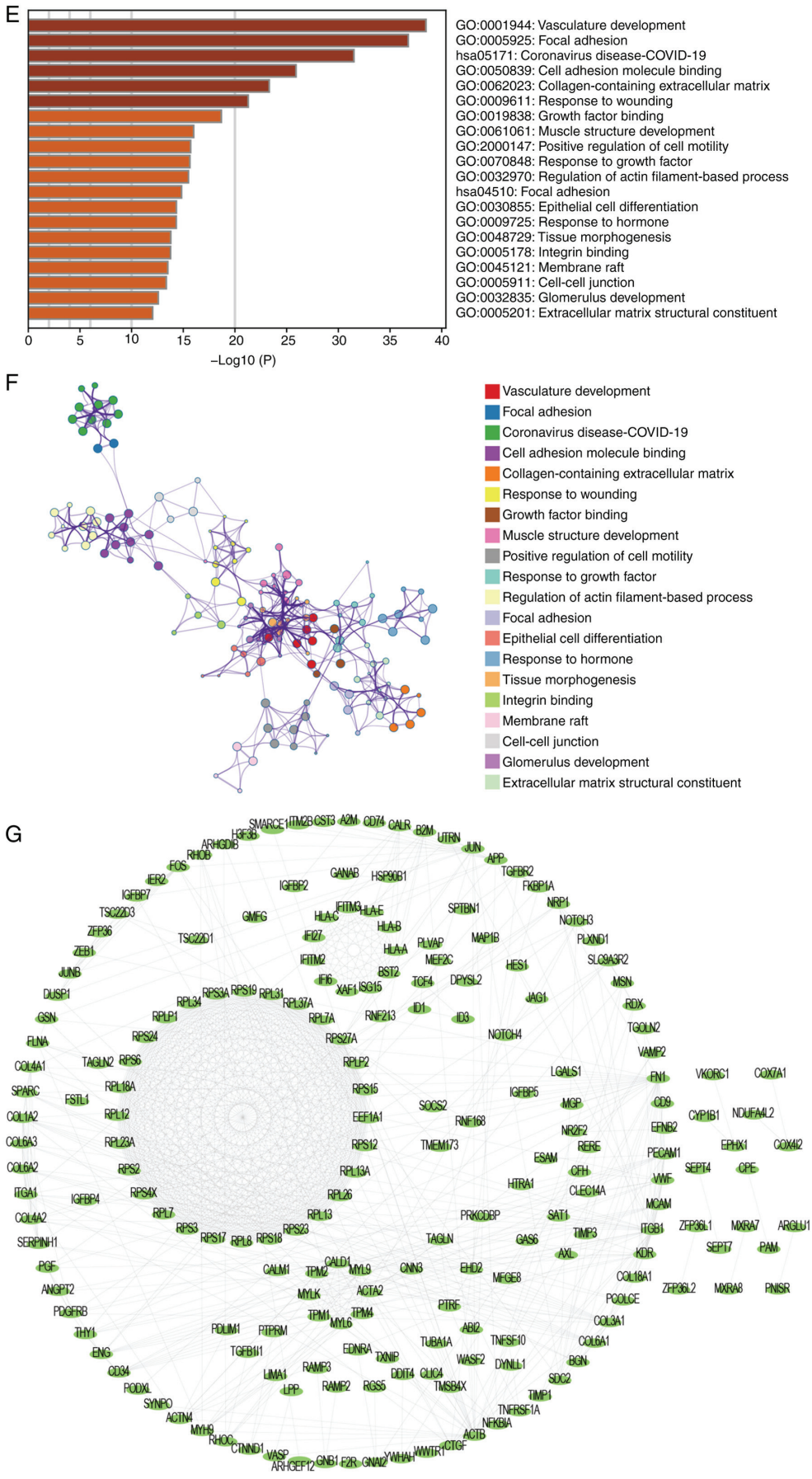

Figure 2. Analysis of receptor-ligand relationships, enriched pathways and protein-protein interaction of key genes (GSE138433 dataset). (A) Representative ligand-receptor pairs. (B) Interactions of ligand-receptor pairs in different cell category. (C) Pathways related to cell-cell communication. (D) Number of ligand-receptor gene pairs corresponding to each cell group. (F and E) Enriched pathway analysis of the identified marker genes. (G) Protein-protein interaction network. CC, cellular component; GO, Gene Ontology; NES, normalized enrichment score; NK, natural killer.

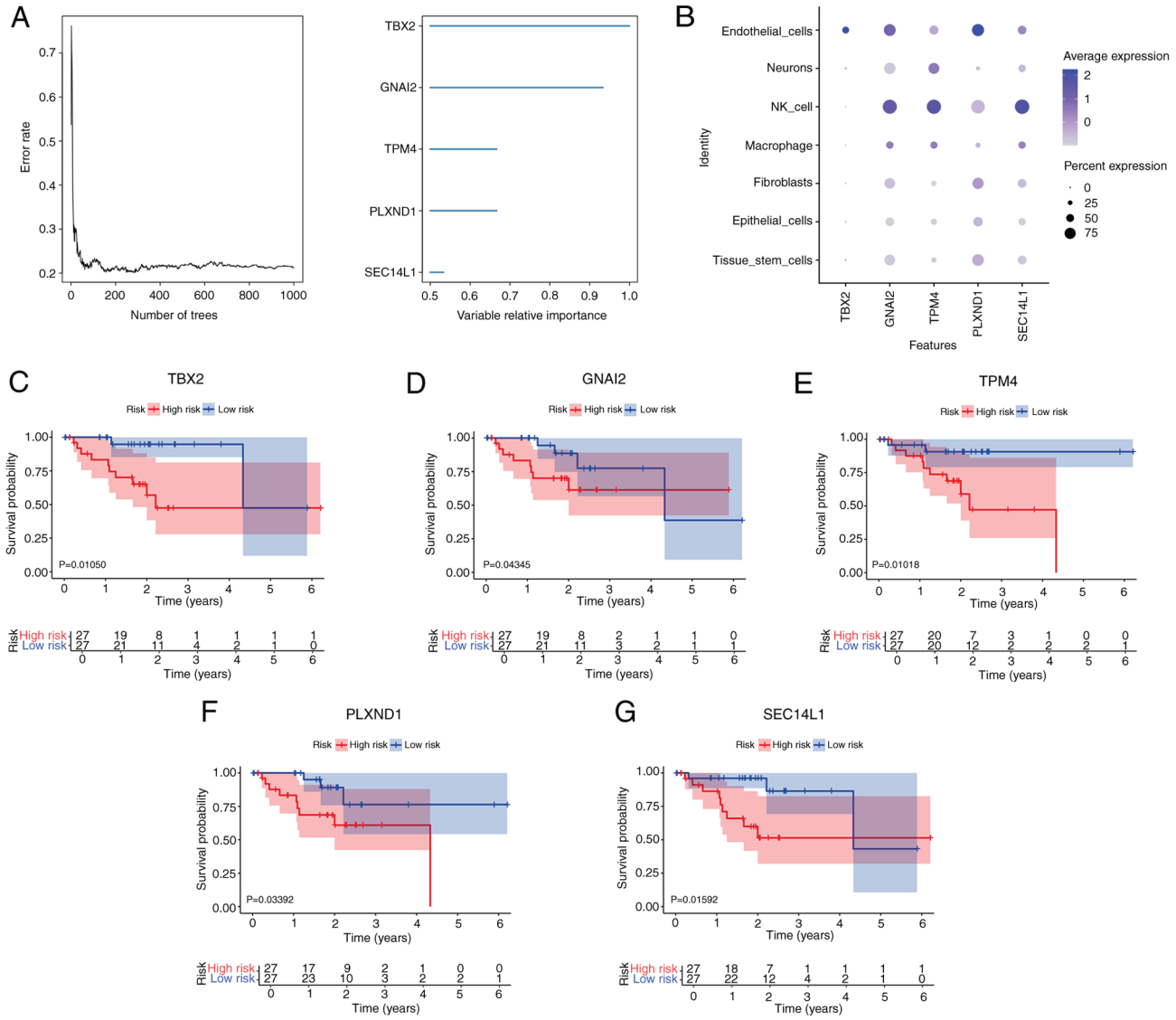

Figure 3. Random survival forest analysis of marker genes (TCGA-UVM dataset). (A) Random survival forest analysis and 5 genes with a relative importance of >0.5. (B) The expression levels of key genes in different cell clusters. Survival curves for (C) *TBX2*, (D) *GNAI2*, (E) *TPM4*, (F) *PXLND1* and (G) *SEC14L1* in The Cancer Genome Atlas-uveal melanoma cohort. The P-value of the two-stage weighted test of each gene is shown. GNAI2, G protein subunit α I2; NK, natural killer; PLXND1, plexin D1; SEC14L1, SEC14-like lipid binding 1; TBX2, T-Box transcription factor 2; TPM4, tropomyosin 4.

(P<0.01; Fig. 4C). *TBX2* expression was most significantly positively correlated with resting CD4 memory T cells and negatively correlated with M0 macrophages (both P<0.01; Fig. 4C). Correlations were also observed between these key genes and different immune factors, including immune modulators, chemokines, major histocompatibility complex and cell receptors based on the TISIDB database (Fig. 4D). Notably, the expression level of *TPM4* was significantly positively correlated with almost all immune factors. By contrast, the expression level of *PLXND1* was negatively correlated with most immune factors.

Analysis of tumor immune dysfunction and exclusion showed differences between the high and low expression groups (with the median value as the cut-off for grouping). A significant difference in the dysfunction level between the high and low expression groups was only found for *GNAI2* (P<0.001; Fig. 5A). In the exclusion and dysfunction analyses, the H-score group referred to samples with scores higher than the median score and the L-score group referred to samples with scores lower than the median score.

With respect to the relationship between key genes and the sensitivity to common chemotherapy drugs, the expression levels of the key genes were significantly correlated with sensitivity to bexarotene, bicalutamide, docetaxel, bryostatin.1, JNK inhibitor VIII, lenalidomide, mitomycin C and sunitinib (Fig. S3).

Specific signaling pathways associated with key genes. Certain highly significant pathways enriched in the key genes are shown in Fig. 6. The *GNAI2* gene was enriched in pathways such as 'chromosome organization involved in meiotic cell cycle' and 'high density lipoprotein particle assembly' in the GO analysis and in pathways such as 'acute myeloid leukemia' and 'basal cell carcinoma' in the KEGG analysis (Fig. 6A and B). The *PLXND1* gene was enriched in pathways such as 'growth plate cartilage chondrocyte differentiation' and 'positive regulation of oxidative stress induced cell death'

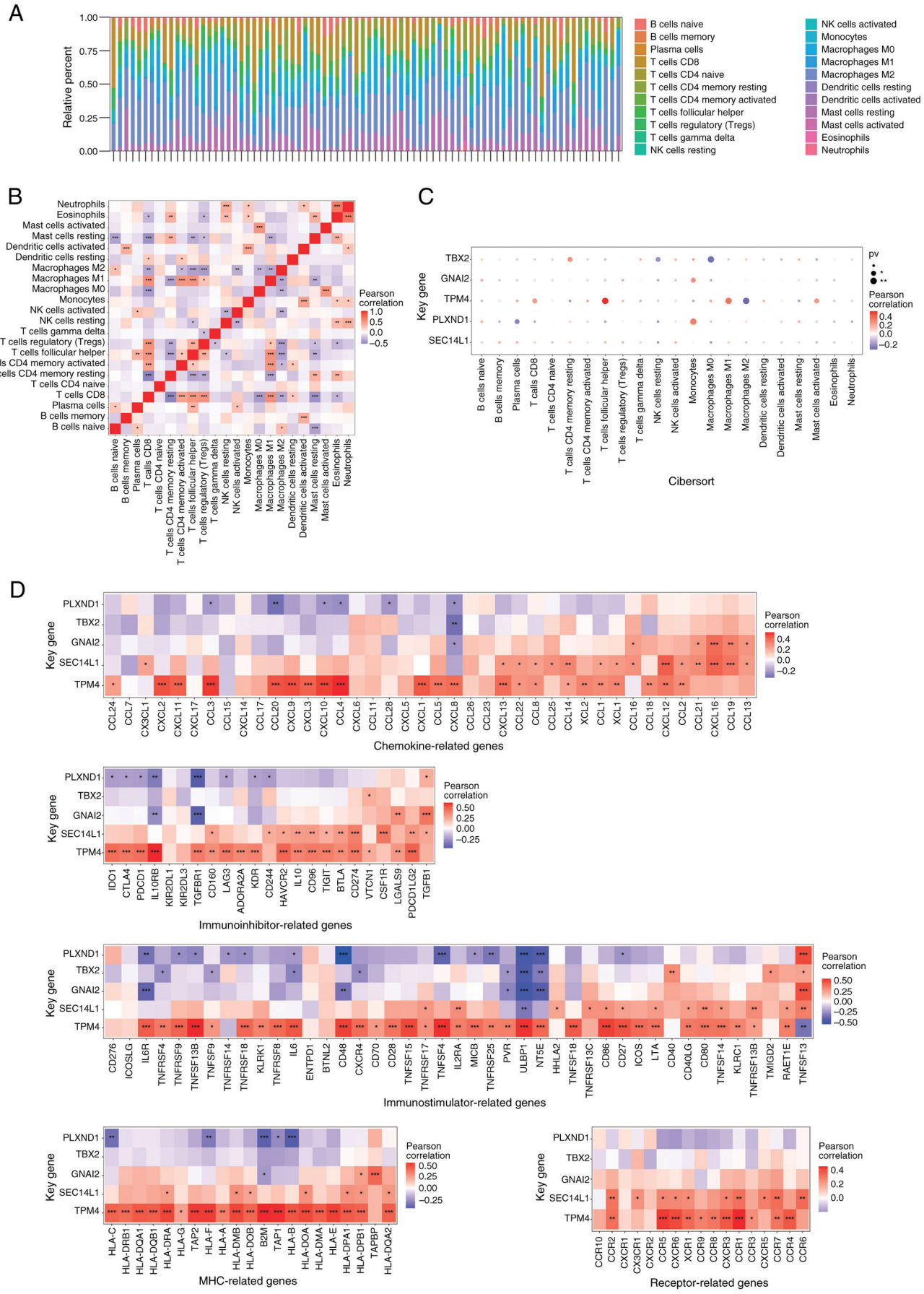

Figure 4. Immune infiltration in uveal melanoma (TCGA-UVM dataset). (A) Immune cell content of each sample. (B) Immune cell correlation map. (C) Relationship between key genes and immune cells. (D) Correlations between key genes and immune-factor (chemokines, immunoinhibitors, immunostimulators, MHC and receptors) related genes. GNAI2, G protein subunit α I2; MHC, major histocompatibility complex; NK, natural killer; PLXND1, plexin D1; pv, P-value; SEC14L1, SEC14-like lipid binding 1; TBX2, T-Box transcription factor 2; TPM4, tropomyosin 4.

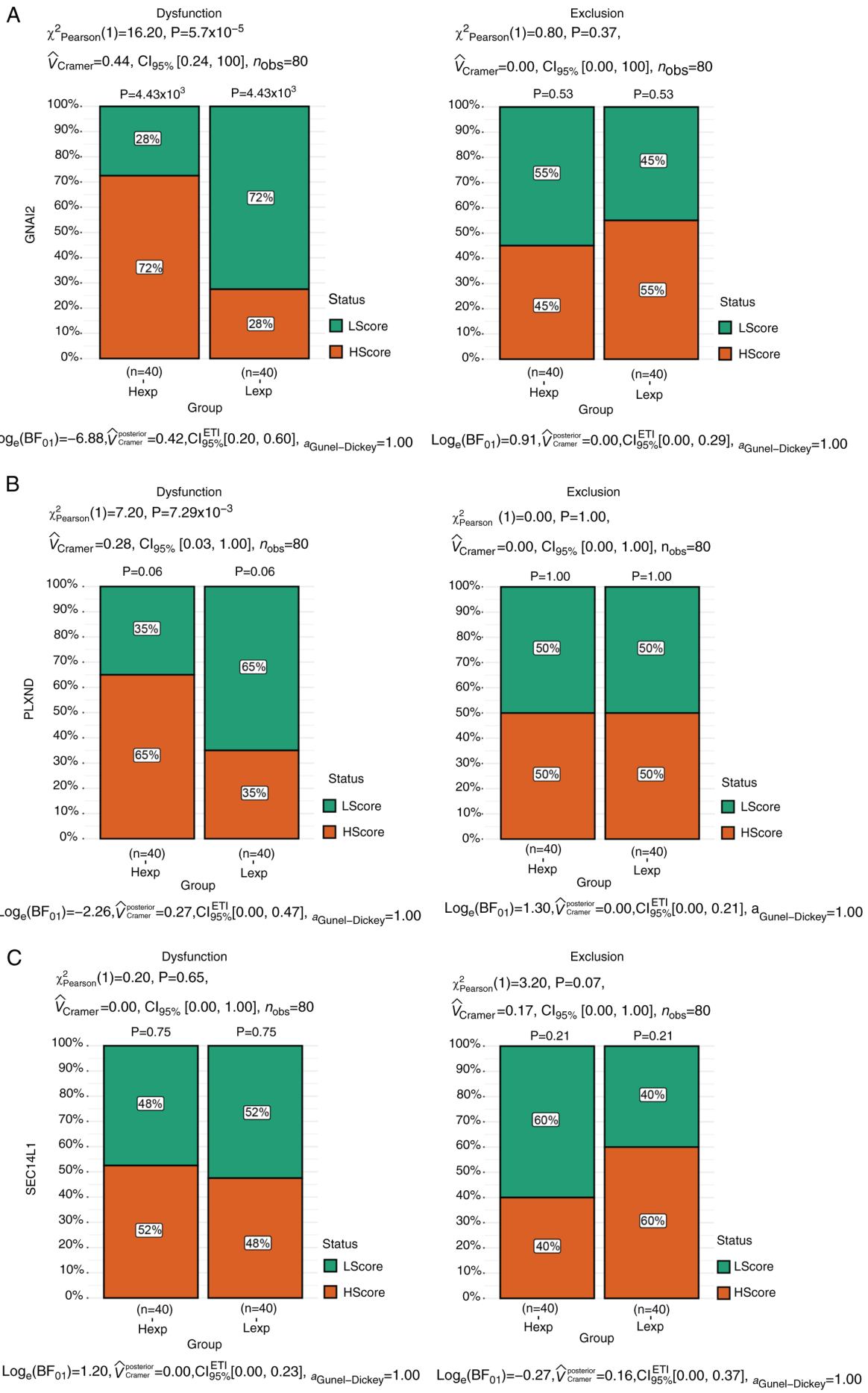

Figure 5. Continued.

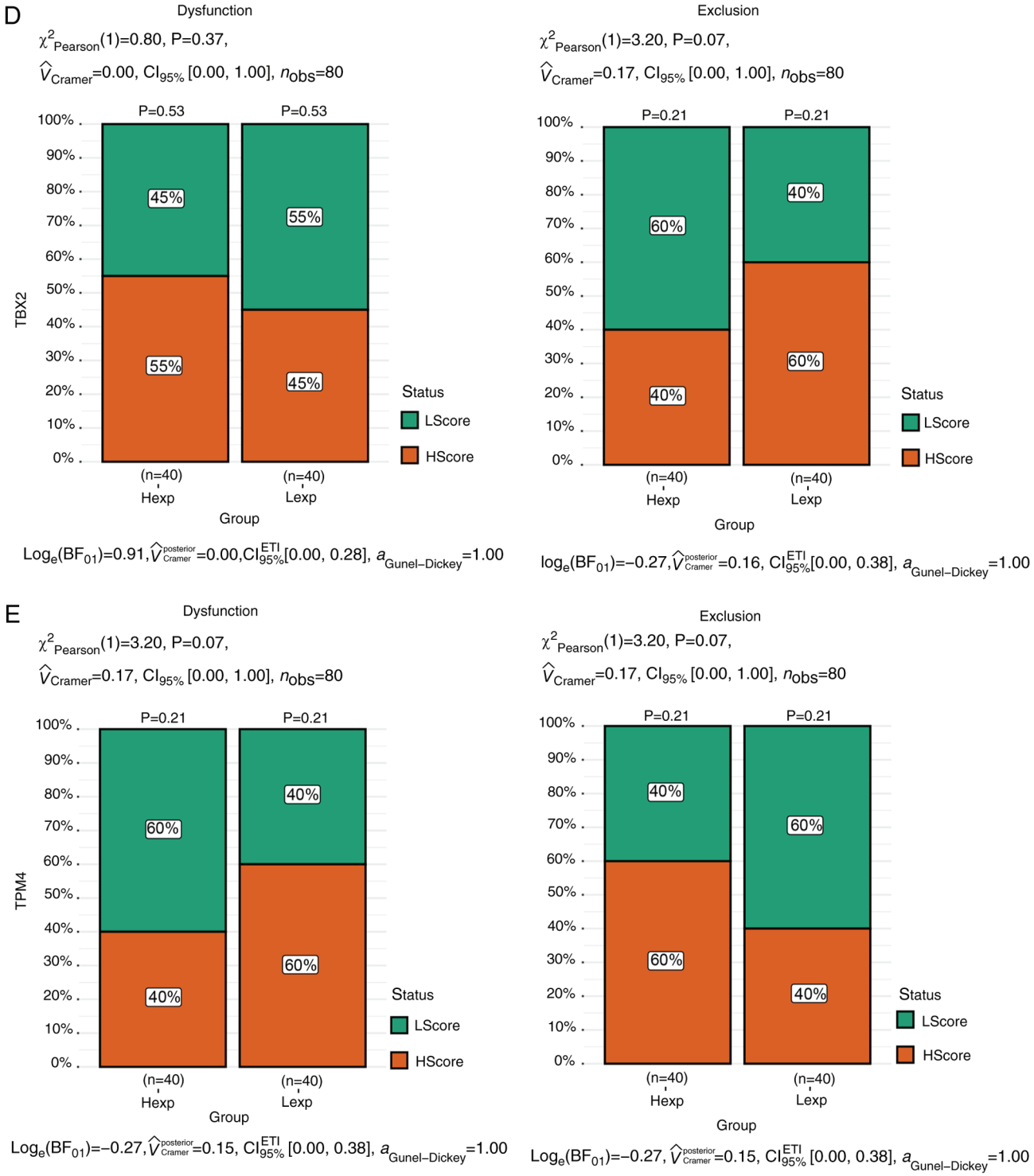

Figure 5. Analysis of tumor immune dysfunction and exclusion of key genes (TCGA-UVM dataset). Dysfunction and Exclusion of (A) *GNAI2*, (B) *PLXND1*, (C) *SEC14L1*, (D) *TBX2* and (E) *TPM4*. GNAI2, G protein subunit α I2; PLXND1, plexin D1; SEC14L1, SEC14-like lipid binding 1; TBX2, T-Box transcription factor 2; TPM4, tropomyosin 4.

in the GO analysis and in pathways such as 'basal cell carcinoma' and 'cell cycle' in the KEGG analysis (Fig. 6C and D). The *SEC14L1* gene was enriched in pathways such as 'aerobic electron transport chain' and 'ATP synthesis coupled electron transport' in the GO analysis and in pathways such as 'acute myeloid leukemia' and 'glycosaminoglycan biosynthesis chondroitin sulfate' in the KEGG analysis (Fig. 6E and F). The *TBX2* gene was enriched in pathways such as 'establishment of protein localization to chromosome' and 'formation of extrachromosomal circular DNA' in the GO analysis and in pathways such as 'glyoxylate and dicarboxylate metabolism' and 'histidine metabolism' in the KEGG analysis (Fig. 6G and H). The *TPM4* gene was enriched in pathways such as 'cell redox homeostasis' and 'cellular response to ionizing radiation' in the GO analysis and in pathways such as 'cytosolic DNA sensing pathway' and 'drug metabolism cytochrome P450' in

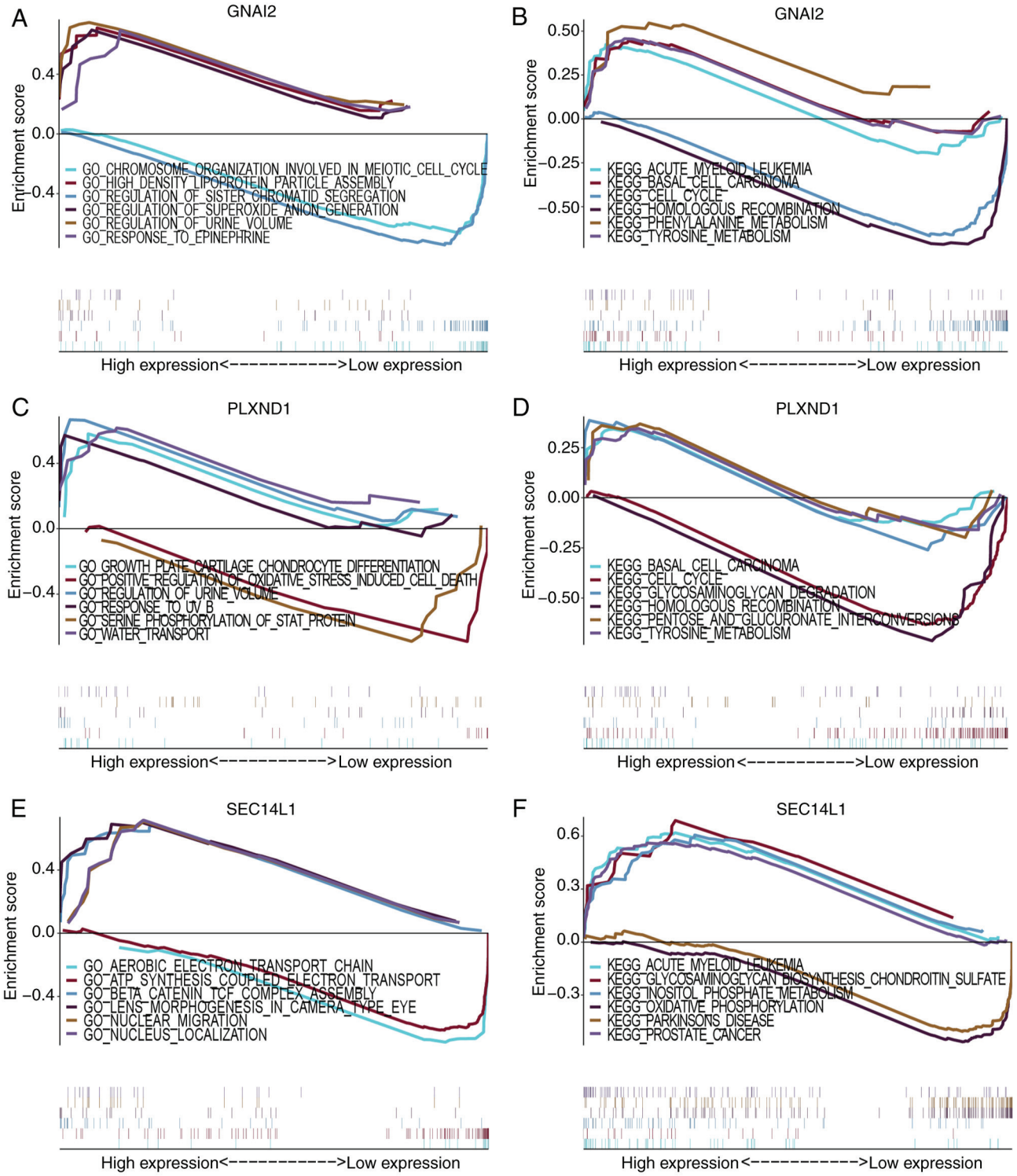

Figure 6. Continued.

the KEGG analysis (Fig. 6I and J). These signaling pathways influenced the progression of UM.

Performance of the nomogram and calibration curve. The expression levels of key genes were visualized in the form of column charts based on the results of the regression analysis. Regression analysis showed that the values of different clinical indicators of UM and the expression distribution of key genes contributed to the scoring process to varying degrees in all samples (Fig. 7A). Furthermore, predictive analysis was performed for 1-year and 2-year survival periods, and the predicted OS rate aligned well with the observed OS (Fig. 7B). However, the predicted OS rate for the 3-year and 5-year period was not constructed due to the poor curve fitting (Fig. S4).

Correlations between the expression levels of the key genes and UM-related genes. A total of 2,312 disease-related genes associated with UM were obtained from the GeneCards

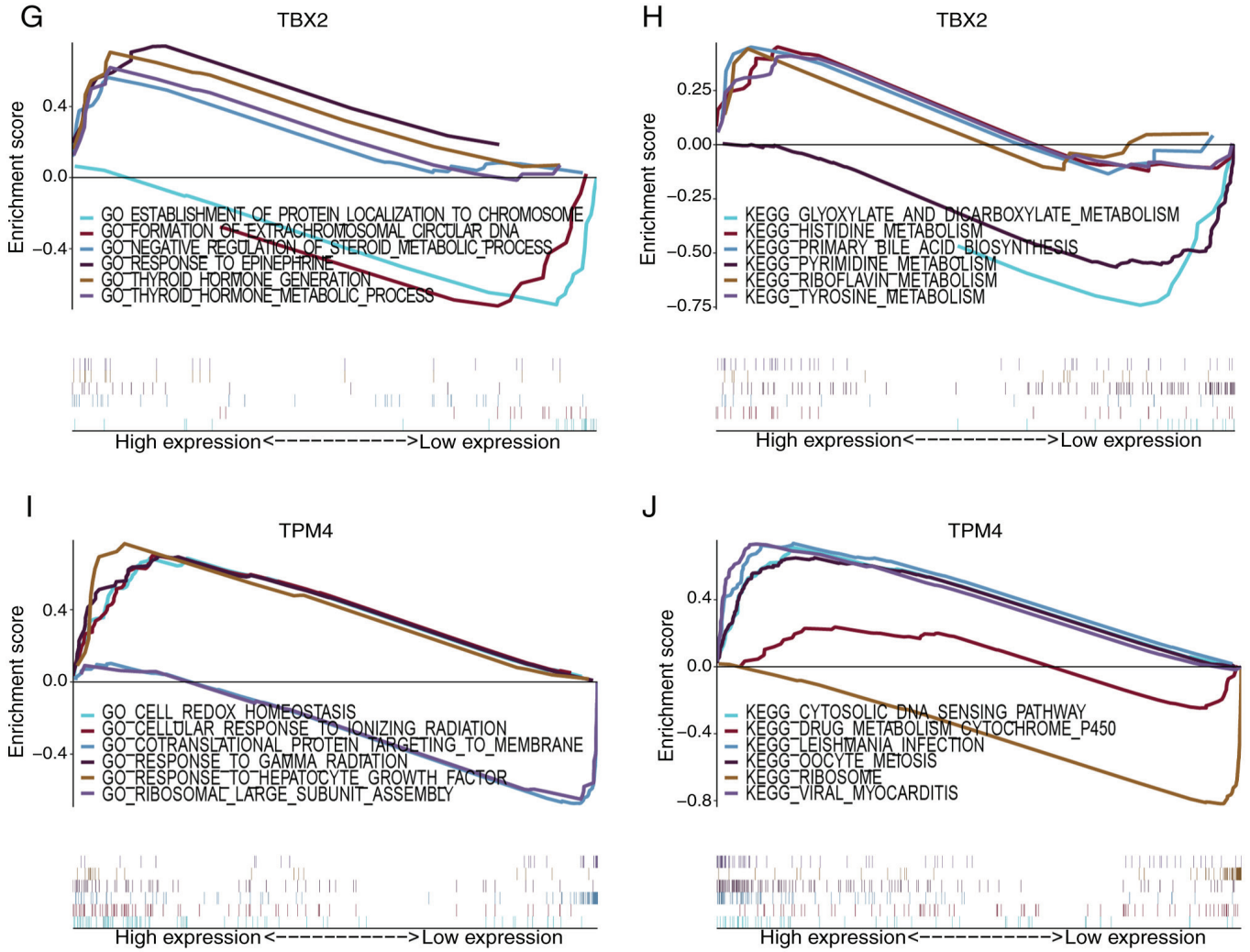

Figure 6. Specific signaling pathways enriched by key genes. GO and KEGG analysis of (A and B) *GNAI2*, (C and D) *PLXND1*, (E and F) *SEC14L1*, (G and H) *TBX2* and (I and J) of *TPM4*. GNAI2, G protein subunit α I2; GO, Gene Ontology; KEGG, Kyoto Encyclopedia of Genes and Genomes; PLXND1, plexin D1; SEC14L1, SEC14-like lipid binding 1; TBX2, T-Box transcription factor 2; TPM4, tropomyosin 4.

database. Analysis of the expression levels of the 5 key genes in different clusters (Fig. 8A) and the expression levels of the top 20 disease-related genes, based on their relevance scores from the GeneCards database, (Fig. 8B and C) showed a significant correlation between the expression levels of the key genes and multiple UM-related genes (Fig. 8D). Notably, the expression level of *TPM4* had a significant positive correlation with that of melanocortin 1 receptor (r=0.613, P<0.001; Fig. 8D), and the expression level of *GNAI2* had a significant negative correlation with that of protection of telomeres protein 1 (r=-0.601, P<0.001; Fig. 8D). The correlations of *TPM4* and UM-related genes were mostly opposite to that of *GNAI2* and UM-related genes (Fig. 8D). However, the correlations of *PLXND1* and *GNAI2* with UM-related genes were more consistent (Fig. 8D). Additionally, when the expression of key and UM-related genes were analyzed at the single-cell level, these key genes were co-expressed with a number of UM-related genes (Fig. S5).

ceRNA network analysis of the key genes. First, extracting mRNA-miRNA interaction pairs related to the 5 key mRNAs from the miRWalk database resulted in 1,414 miRNAs. Only 41 mRNA-miRNA interaction pairs that were detectable in both the TargetScan and miRDB databases (including 4 mRNAs and 11 miRNAs) were then retained. Based on these miRNAs, the interacting lncRNAs were further predicted, resulting in 2,936 predicted interaction pairs (including 11 miRNAs and 1,071 lncRNAs). Finally, a ceRNA network, which involved 4 mRNAs and 11 miRNAs (Fig. 9) with 1,071 lncRNAs (Fig. S6), was constructed using Cytoscape.

In vitro biofunction of PLXND1 and GNAI2 in C918 cells. Firstly, the endogenous transcription level of feature genes in C918 cells were tested. The mean quantification cycle values of *PLXND1, TBX2, SEC14L1, GNAI2* and *TPM4* were 25.3, 32.3, 25.1, 22.2, and 23.2, respectively (Fig. S7A). *TBX2* was excluded from the subsequent siRNA knockdown experiments owing to its low native expression, with a CT >30 compared with *GAPDH* (P<0.0001; Fig. S7A). *SEC14L1* and *TPM4* were also not tested in the further experiments due to the low knockdown efficiency (<50%) of the respective siRNAs compared with the negative control (P<0.01 and P<0.001, respectively; Fig. S7D and E). The *PLXND1* and *GNAI2* siRNAs were selected for CCK-8 and gap closure assays due to their high silencing efficiencies (>50%; Fig. S7B and C).

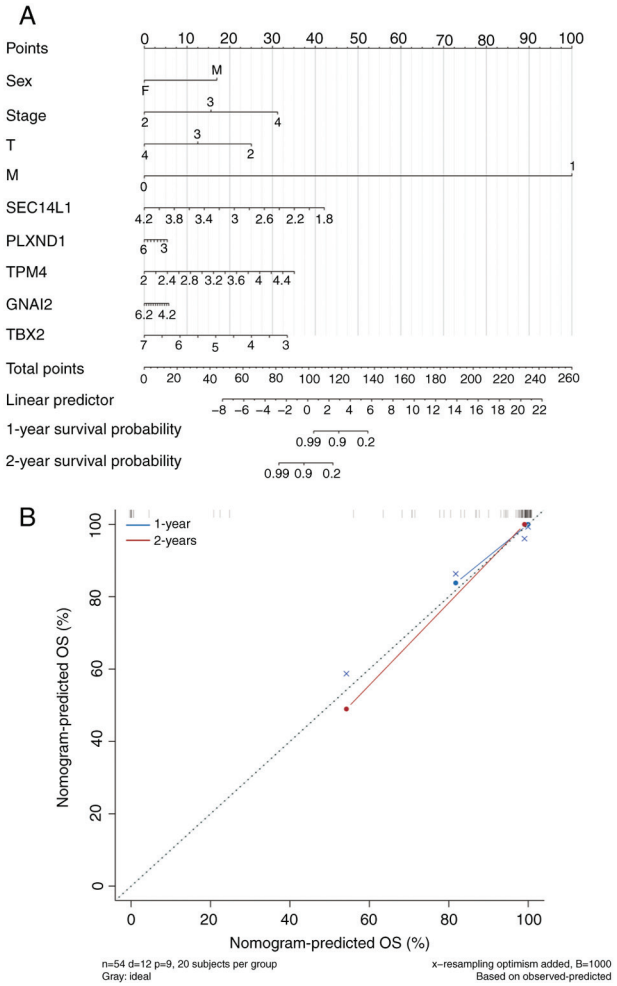

Figure 7. Construction of a nomogram and calibration curve. (A) Regression analysis of different clinical indicators and the expression distribution of key genes. (B) Predictive analysis of the 1 and 2-year OS periods. GNAI2, G protein subunit α I2; M, metastasis stage; OS, overall survival; PLXND1, plexin D1; SEC14L1, SEC14-like lipid binding 1; T, tumor stage; TBX2, T-Box transcription factor 2; TPM4, tropomyosin 4.

The cell viabilities of the *PLXND1* and *GNAI2* knockdown groups were 59.8% and 62.1%, respectively, which were significantly lower than those of the siRNA control group (both P<0.0001; Fig. 10A and B). In the gap closure assay, the closure rate was significantly lower in the *PLX1* (70.3%; P<0.001; Fig. 10D) and *GNAI2* (68.7%; P<0.01; Fig. 10C) knockdown groups compared with the control group (92.9%). Representative images of the gap closure assay are shown in Fig. 10E.

Discussion

The present study, by analyzing single-cell data and annotating endothelial cells, showed that endothelial cells exhibited the most extensive cellular communication. Notably, these cells had significant roles in various biological processes in UM, particularly in vascular development. The findings of the present study will not only enhance the understanding of the pathobiology of UM at the cellular level but will also aid in the discovery of novel pathways and therapeutic targets for this malignancy.

Endothelial cells play a crucial role in the development of UM. García-Mulero *et al* (32) used the ESTIMATE algorithm to analyze TCGA data and found a close association among endothelial cells, fibroblasts (stromal cells), immune cells (especially cytotoxic cells) and adverse prognoses from UM recurrence. Although endothelial cells only account for 4-18% of ocular cells (depending on the tissue) (33), they play a pivotal role in UM progression and metastasis by orchestrating intricate interactions within the tumor microenvironment (34). UM arises in highly vascularized tissue, indicating a significant involvement of endothelial cells in its pathogenesis (35). Endothelial cells are key factors of angiogenesis, a process crucial for tumor growth and dissemination. Furthermore, through the secretion of angiocrine factors, endothelial cells not only regulate angiogenesis but also modulate tumor cell behavior, immune response and stromal remodeling (36). The aforementioned findings show that endothelial cells engage in extensive crosstalk with other cell types, including tumor cells, immune cells and fibroblasts, to promote tumor growth, invasion and metastasis. Additionally, endothelial cells may facilitate tumor cell intravasation into the bloodstream by participating in vascular mimicry and interacting with tumor cells during this process (37). The high number of cell communications identified in endothelial cells underscores their essential role in driving UM progression through angiogenesis, microenvironmental interactions and response to pro-angiogenic signals secreted by tumor cells (38). In normal conditions, endothelial cells are situated on the vascular wall and act as barriers preventing cell entry or exit from the bloodstream (38). Epithelial-to-mesenchymal transition (EMT) is a process in which epithelial cells lose cell adhesion and polarity and transform into mesenchymal-like cells (39,40). Vascular endothelial cells also participate in regulating cancer cells, thereby enhancing their invasive and migratory capabilities. A study has indicated that vascular endothelial cells induce EMT in human pancreatic, lung and murine mammary gland cancer cell lines by continuously secreting $TGF\beta_1$ and $TGF\beta_2$ (41). Cancer cells overcome the endothelial barrier by altering their vascular system. During the migration of mesenchymal cancer cells towards blood vessels, they may undergo passive transendothelial migration through endothelial cells owing to the highly leaky nature of tumor vessels (42).

To the best of our knowledge, this is the first study to identify that the *SEC14L1*, *TPM4*, *TBX2*, *PLXND1* and *GNAI2* genes are associated with UM prognosis. The KM survival analysis demonstrated significant differences in the expression levels of these 5 genes between the high and low expression groups in the TCGA-UM cohort. *SEC14L1* has been reported as a prognostic factor in both breast cancer and prostate cancer (43,44). *TPM4* has been reported as a prospective marker for diagnosis, treatment outcome, and a small molecular drugs target for pan-cancer treatment, including in gastric cancer treatment (45). Consistent results were obtained in the present study. *TPM4* expression was positively correlated with almost all immune factors in contrast to that of other genes. This indicated the essential role of *TPM4* in immune infiltration and the progression of UM.

TBX2 and *TBX3,* members of the T-box transcription factor family, are upregulated in various cancer types, including melanoma, breast, liver, lung, pancreatic, ovarian and cervical cancer (46). As the master regulator of the type 1 immune response,

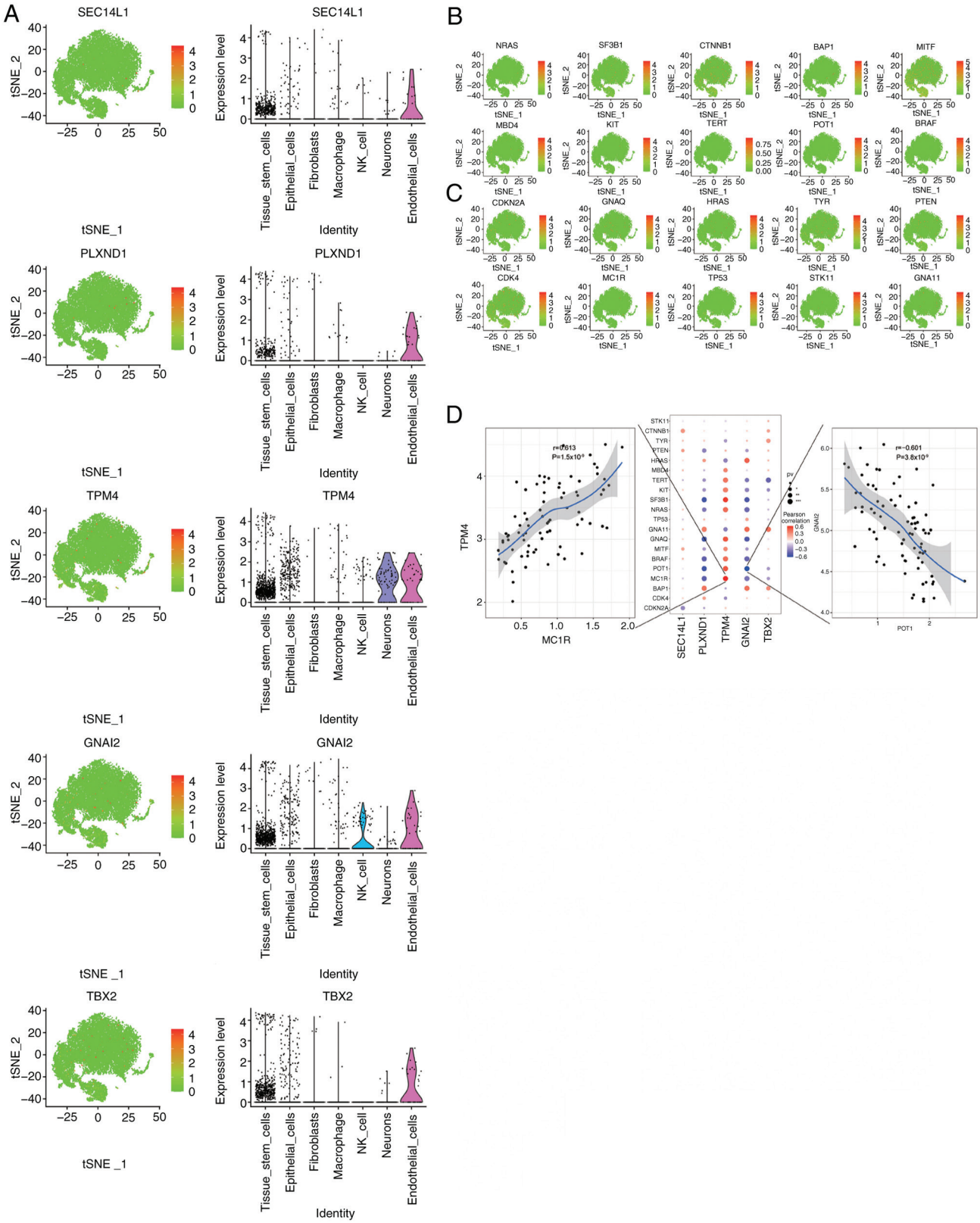

Figure 8. Expression levels of key genes and UM-related genes. (A) The expression levels of 5 key genes in different clusters. (B and C) The expression levels of the top 20 genes based on their relevance scores. (D) The correlations between the expression levels of the key genes and multiple UM-related genes. GNAI2, G protein subunit α I2; NK, natural killer; PLXND1, plexin D1; SEC14L1, SEC14-like lipid binding 1; t-SNE, t-distributed Stochastic Neighbor Embedding; TBX2, T-Box transcription factor 2; TPM4, tropomyosin 4; UV, uveal melanoma.

TBX21 is also upregulated in the leukocytes of peripheral blood in patients with late-onset Alzheimer's disease (47). *PLXND1* knockdown significantly reduces cell migration and invasion and inhibits EMT in colorectal cancer (48). The activation of *PLXND1* in dorsal root ganglion cells increases the migratory and invasive activities of pancreatic cancer cells and a loss of neural *PLXND1*

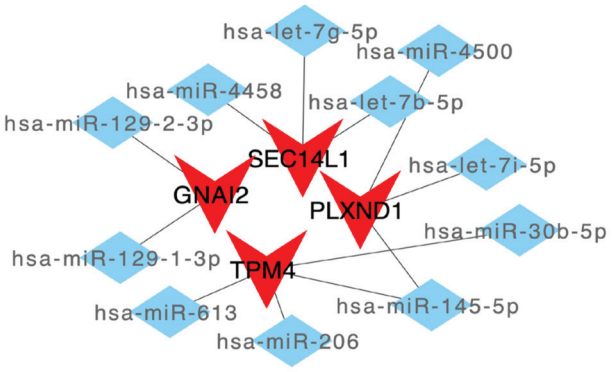

Figure 9. Competing endogenous RNA network of the key genes involved 4 mRNAs and 11 miRNAs. GNAI2, G protein subunit α I2; miR/miRNA, microRNA; PLXND1, plexin D1; SEC14L1, SEC14-like lipid binding 1; TBX2, T-Box transcription factor 2; TPM4, tropomyosin 4.

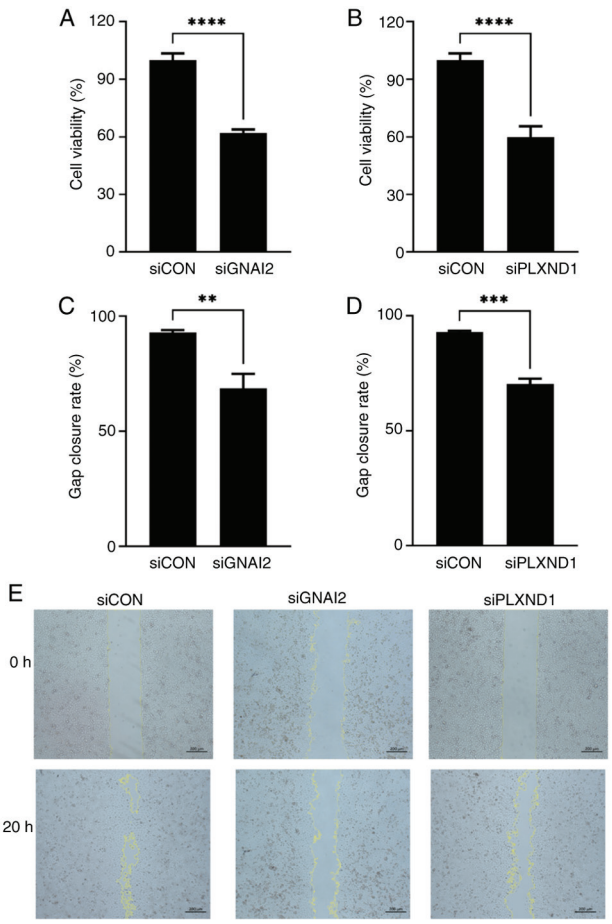

Figure 10. *In vitro* biofunction of *PLXND1* and *GNAI2* in C918 cells. Viability of C918 cells after (A) *GNAI2* and (B) *PLXND1* siRNA transfection. Gap closure rate of the (C) siGNAI2 and (D) siPLX1 groups after 20 h. (E) Representative images of the gap closure assay; scale bar, 200 μm. **P<0.01, ***P<0.001, ****P<0.0001. CON, control; GNAI2, G protein subunit α I2; PLXND1, plexin D1; si, small interfering (RNA).

reduces the innervation of orthotopic pancreatic ductal adenocarcinoma and metastasis in mice (49). In addition, *PLXND1* can impair endocardial endothelial autophagy via mediating calcium dyshomeostasis in atrial fibrillation and is a mechanosensor in endothelial cells (50,51). It is well known that the *GNAQ* and *GNA11* genes are mutated in 80-90% of UM in a mutually exclusive pattern (52). These genes encode the α subunits of the heterotrimeric G proteins, Gq and G11, commonly termed the Gq/11 (Gq/G11) family (52). The typical function of Gq/G11 is to activate intracellular signaling pathways in response to activation of the cell surface G protein-coupled receptors (53,54). However, *GNAI2* encodes the α-2 subunit of guanine nucleotide-binding protein G(i) involved in the regulation of adenylate cyclase and transcriptome in ovarian cancer (55), and is a critical regulator of oncogenesis and an upstream driver of cancer progression in ovarian cancer (56). In addition, a protein biomarker study using liquid biopsy revealed a negative correlation between *GNAI2* and the survival of patients with cholangiocarcinoma (57). The aforementioned findings showed notable differences in the biofunction and encoding proteins between the Gq/G11 family and *GNAI2*. Thus, we consider that the mutation of *GNAI2* is a new variant. Consistently, in the present study, the results of the *in vitro* experiments demonstrated a significant reduction in cell viability and gap closure rate after *PLXND1* and *GNAI2* knockdown. This indicated that *PLXND1* and *GNAI2* may serve as potential diagnostic markers and therapeutic targets for UM. Furthermore, these genes and their co-expressions were significantly correlated with disease-related genes, validating the reliability of the study findings and demonstrating complex genetic interactions in UM.

A crucial aspect addressed in the present study was the strong relationship between the tumor microenvironment and notable aspects of disease understanding, such as diagnosis, survival outcome and treatment sensitivity. Previous studies have shown the abundance of several tumor-infiltrating immune cells, T cells and dendritic cells in UM (58,59). A previous study reported a positive correlation between the risk score of UM and the levels of immune cell infiltration, including $CD4^+$ T cells, B cells, NK cells, dendritic cells and macrophages (60). Notably, the findings of the present study further revealed that certain genes were significantly correlated with specific immune cells; for instance, *PLXND1* was associated with monocytes and *TPM4* was associated with follicular helper T cells. Combined with the significant role of *GNAI2* in immune dysfunction, these findings implied the potential value of key genes in UM immunotherapy. Examining the molecular landscape of a disease can significantly contribute to refining current methods and strengthening individualized medicine (61). This underscores that personalized medicine is the future of disease treatment in a world where generalized treatments are becoming less desirable and effective. Furthermore, the accurate prediction of the 1 and 2-year OS rate using key genes and clinical information in the present study illustrated the clinical value of these key genes in predicting the prognosis of patients with UM.

Recent experimental evidence suggests that lncRNAs serve as ceRNAs, bind to miRNAs to modulate miRNA-induced gene silencing, act as natural miRNA sponges, regulate gene expression and play crucial roles in human diseases including UM (62-64). In the present study, a ceRNA network specific for UM was constructed. The findings highlighted the complex nature of UM, combining with the functional roles of various mRNAs, miRNAs and lncRNAs. The intricate network of these molecules along with the heterogeneous nature of the disease presents a challenging scenario for the design of therapeutic strategies. Thus, in the present study, the

cell communication mechanisms among UM were initially elucidated using single-cell and TCGA data and key genes associated with prognosis were identified. Although the present study has reported notable findings, it also has limitations, particularly the lack of *in vivo* verification and examination of detailed molecular mechanisms. Further research is needed to elucidate the molecular mechanisms of UM.

In summary, the results of the present study revealed the communication between endothelial cells and other cell types, elucidating the molecular mechanisms underlying UM. The identification of key genes (*SEC14L1, PLXND1, TPM4, GNAI2* and *TBX2*) in UM prompted further analyses. *In vitro* assays confirmed the functional significance of *PLXND1* and *GNAI2*, with the knockdown of these genes decreasing cell viability and delaying cell migration. We consider that these findings will not only enhance the understanding of the pathobiology of UM at the cellular level but will also serve to reveal novel pathways and therapeutic targets in the treatment of this mucosal cancer.

Acknowledgements

Not applicable.

Funding

The present study was sponsored by the National Natural Science Foundation of China (grant nos. 82201147 and 82171020).

Availability of data and materials

The data generated in the present study may be requested from the corresponding author.

Authors' contributions

NL contributed to investigation (bioinformatics analysis), writing (original draft) and validation (bioinformatics database). JW contributed to investigation (bioinformatics database), writing (original draft) and formal analysis. YD contributed to investigation (*in vitro* experiments) and writing (original draft). YF, ZL and JG contributed to formal analysis and validation (bioinformatics analysis). JC contributed to conceptualization and supervision. JX contributed to conceptualization, writing (review and editing), supervision and funding acquirement. All authors read and approved to the final version of the manuscript. NL, JW and JC confirm the authenticity of all the raw data.

Ethics approval and consent to participate

All experiments were performed in compliance with the Association for Research in Vision and Ophthalmology, and the experimental protocols were evaluated and approved by the Ethical Committee of Eye and ENT Hospital, Fudan University (Shanghai, China; approval no. ky2012-037).

Patient consent for publication

Not applicable.

Competing interests

The authors declare that they have no competing interests.

References

1. McLaughlin CC, Wu XC, Jemal A, Martin HJ, Roche LM and Chen VW: Incidence of noncutaneous melanomas in the U.S. Cancer 103: 1000-1007, 2005.
2. Shields CL, Furuta M, Thangappan A, Nagori S, Mashayekhi A, Lally DR, Kelly CC, Rudich DS, Nagori AV, Wakade OA, *et al*: Metastasis of uveal melanoma millimeter-by-millimeter in 8033 consecutive eyes. Arch Ophthalmol 127: 989-998, 2009.
3. Damato B: Ocular treatment of choroidal melanoma in relation to the prevention of metastatic death-A personal view. Prog Retin Eye Res 66: 187-199, 2018.
4. Damato B, Eleuteri A, Azzam FGT and Coupland SE: Estimating prognosis for survival after treatment of choroidal melanoma. Prog Retina Eye Res 30: 285-295, 2011.
5. Sun S, Shi R, Xu L and Sun F: Identification of heterogeneity and prognostic key genes associated with uveal melanoma using single-cell RNA-sequencing technology. Melanoma Res 32: 18-26, 2022.
6. Eskelin S, Pyrhönen S, Summanen P, Hahka-Kemppinen M and Kivel T: Tumor doubling times in metastatic malignant melanoma of the uvea: Tumor progression before and after treatment. Ophthalmology 107: 1443-1449, 2000.
7. Hou C, Xiao L, Ren X, Tang F, Guo B, Zeng W, Liang C and Yan N: Mutations of GNAQ, GNA11, SF3B1, EIF1AX, PLCB4 and CYSLTR in uveal melanoma in Chinese patients. Ophthalmic Res 63: 358-368, 2020.
8. Robertson AG, Shih J, Yau C, Gibb EA, Oba J, Mungall KL, Hess JM, Uzunangelov V, Walter V, Danilova L, *et al*: Integrative analysis identifies four molecular and clinical subsets in uveal melanoma. Cancer Cell 32: 204-220, 2017.
9. Gupta MP, Lane AM, Deangelis MM, Mayne K, Crabtree M, Gragoudas ES and Kim IK: Clinical characteristics of uveal melanoma in patients with germline BAP1 mutations. JAMA Ophthalmol 133: 881-887, 2015.
10. Jager MJ, Ly LV, El Filali M and Madigan MC: Macrophages in uveal melanoma and in experimental ocular tumor models: Friends or foes? Prog Retin Eye Res 30: 129-146, 2011.
11. Rossi E, Schinzari G, Zizzari IG, Maiorano BA, Pagliara MM, Sammarco MG, Fiorentino V, Petrone G, Cassano A, Rindi G, *et al*: Immunological backbone of uveal melanoma: Is there a rationale for immunotherapy? Cancers (Basel) 11: 1055, 2019.
12. Zhang Y, Wang D, Peng M, Tang L, Ouyang J, Xiong F, Guo C, Tang Y, Zhou Y, Liao Q, *et al*: Single-cell RNA sequencing in cancer research. J Exp Clin Cancer Res 40: 81, 2021.
13. Pandiani C, Strub T, Nottet N, Cheli Y, Gambi G, Bille K, Husser C, Dalmasso M, Béranger G, Lassalle, S, *et al*: Single-cell RNA sequencing reveals intratumoral heterogeneity in primary uveal melanomas and identifies HES6 as a driver of the metastatic disease. Cell Death Differ 28: 1990-2000, 2021.
14. Durante MA, Rodriguez DA, Kurtenbach S, Kuznetsov JN, Sanchez MI, Decatur CL, Snyder H, Feun LG, Livingstone AS and Harbour JW: Single-cell analysis reveals new evolutionary complexity in uveal melanoma. Nat Commun 11: 496, 2020.
15. Schwager SC, Taufalele PV and Reinhart-King CA. Cell-cell mechanical communication in cancer. Cell Mol Bioeng 12: 1-14, 2019.
16. Bai H, Bosch JJ and Heindl LM: Current management of uveal melanoma: A review. Clin Exp Ophthalmol 51: 484-494, 2023.
17. Kaštelan S, Antunica AG, Oresković LB, Pelčić G, Kasun E and Hat K: Immunotherapy for uveal melanoma-Current knowledge and perspectives. Curr Med Chem 27: 1350-1366, 2020.
18. Oliva M, Rullan AJ and Piulats JM: Uveal melanoma as a target for immune-therapy. Ann Transl Med 4: 172, 2016.
19. Tomczak K, Czerwińska P and Wiznerowicz M: The cancer genome atlas (TCGA): An immeasurable source of knowledge. Contemp Oncol (Pozn) 19: A68-A77, 2015.
20. Weinstein JN, Collisson EA, Mills GB, Shaw KR, Ozenberger BA, Ellrott K, Shmulevich I, Sander C and Stuart JM; Cancer Genome Atlas Research Network: The cancer genome atlas pan-cancer analysis project. Nat Genet 45: 1113-1120, 2013.
21. Davis S and Meltzer PS: GEOquery: A bridge between the gene expression omnibus (GEO) and bioconductor. Bioinformatics 23: 1846-1847, 2007.

22. Hao Y, Hao S, Andersen-Nissen E, Mauck WM III, Zheng S, Butler MJ, Lee A, Wilk AJ, Darby C, Zager M, *et al*: Integrated analysis of multimodal single-cell data. Cell 184: 3573-3587.e29, 2021.
23. Garcia-Alonso L, Lorenzi V, Mazzeo CI, Alves-Lopes JP, Roberts K, Sancho-Serra C, Engelbert J, Marečková M, Gruhn WH, Botting RA, *et al*: Single-cell roadmap of human gonadal development. Nature 607: 540-547, 2022.
24. Efremova M, Vento-Tormo M, Teichmann SA and Vento-Tormo R: CellPhoneDB: Inferring cell-cell communication from combined expression of multi-subunit ligand-receptor complexes. Nat Protoc 15: 1484-1506, 2020.
25. Yu G, Wang LG, Han Y and He QY: ClusterProfiler: An R package for comparing biological themes among gene clusters. OMICS 16: 284-287, 2012.
26. Shannon P, Markiel A, Ozier O, Baliga NS, Wang JT, Ramage D, Amin N, Schwikowski B and Ideker T: Cytoscape: A software environment for integrated models of biomolecular interaction networks. Genome Res 13: 2498-2504, 2003.
27. Ishwaran H, Kogalur UB, Blackstone EH and Lauer MS: Random survival forests. 2008.
28. Newman AM, Steen CB, Liu CL, Gentles AJ, Chaudhuri AA, Scherer F, Khodadoust MS, Esfahani MS, Luca BA, Steiner D, *et al*: Determining cell type abundance and expression from bulk tissues with digital cytometry. Nat Biotechnol 37: 773-782, 2019.
29. Li H, Han D, Hou Y, Chen H and Chen Z: Statistical inference methods for two crossing survival curves: A comparison of methods. PLoS One 10: e0116774, 2015.
30. Livak KJ and Schmittgen TD: Analysis of relative gene expression data using real-time quantitative PCR and the 2(-Delta Delta C(T)) Method. Methods 25: 402-408, 2001.
31. Neophytou CM, Panagi M, Stylianopoulos T and Papageorgis P: The role of tumor microenvironment in cancer metastasis: Molecular mechanisms and therapeutic opportunities. Cancers (Basel) 13: 2053, 2021.
32. García-Mulero S, Alonso MH, Del Carpio LP, Sanz-Pamplona R and Piulats JM: Additive role of immune system infiltration and angiogenesis in uveal melanoma progression. Int J Mol Sci 22: 2669, 2021.
33. Voigt AP, Mullin NK, Stone EM, Tucker BA, Scheetz TE and Mullins RF: Single-cell RNA sequencing in vision research: Insights into human retinal health and disease. Prog Retin Eye Res 83: 100934, 2021.
34. Castet F, Garcia-Mulero S, Sanz-Pamplona R, Cuellar A, Casanovas O, Caminal JM and Piulats JM: Uveal melanoma, angiogenesis and immunotherapy, is there any hope? Cancers (Basel) 11: 834, 2019.
35. Notting IC, Missotten GS, Sijmons B, Boonman ZF, Keunen JE and van der Pluijm G: Angiogenic profile of uveal melanoma. Curr Eye Res 31: 775-785, 2006.
36. Potente M and Mäkinen T: Vascular heterogeneity and specialization in development and disease. Nat Rev Mol Cell Biol 18: 477-494, 2017.
37. Hanahan D and Weinberg RA: Hallmarks of cancer: The next generation. Cell 144: 646-674, 2011.
38. Krüger-Genge A, Blocki A, Franke RP and Jung F: Vascular endothelial cell biology: An update. Int J Mol Sci 20: 4411, 2019.
39. Thiery JP, Acloque H, Huang RY and Nieto MA: Epithelial-mesenchymal transitions in development and disease. Cell 139: 871-890, 2009.
40. Nieto MA: The ins and outs of the epithelial to mesenchymal transition in health and disease. Annu Rev Cell Dev Biol 27: 347-376, 2011.
41. Kimura C, Hayashi M, Mizuno Y and Oike M: Endothelium-dependent epithelial-mesenchymal transition of tumor cells: Exclusive roles of transforming growth factor β1 and β2. Biochim Biophys Acta 1830: 4470-4481, 2013.
42. Shenoy AK and Lu J: Cancer cells remodel themselves and vasculature to overcome the endothelial barrier. Cancer Lett 380: 534-544, 2016.
43. Sonbul SN, Aleskandarany MA, Kurozumi S, Joseph C, Toss MS, Diez-Rodriguez M, Diez-Rodriguez M, Nolan CC, Mukherjee A, Martin S, *et al*: Saccharomyces cerevisiae-like 1 (SEC14L1) is a prognostic factor in breast cancer associated with lymphovascular invasion. Mod Pathol 31: 1675-1682, 2018.
44. Agell L, Hernández S, Nonell L, Lorenzo M, Puigdecanet E, de Muga S, Juanpere N, Bermudo R, Fernández PL, Lorente JA, *et al*: A 12-gene expression signature is associated with aggressive histological in prostate cancer: SEC14L1 and TCEB1 genes are potential markers of progression. Am J Pathol 181: 1585-1594, 2012.
45. Guo Q, Zhao L, Yan N, Li Y, Guo C, Dang S, Shen X, Han J and Luo Y: Integrated pan-cancer analysis and experimental verification of the roles of tropomyosin 4 in gastric cancer. Front Immunol 14: 1148056, 2023.
46. Lu J, Li XP, Dong Q, Kung HF and He ML: TBX2 and TBX3: The special value for anticancer drug targets. Biochim Biophys Acta 1806: 268-274, 2010.
47. Fatemi Langroudi SR, Zeinaly M and Ajamian F: TBX21, the Master regulator of the type 1 immune response, overexpresses in the leukocytes of peripheral blood in patients with late-onset Alzheimer's disease. Immun Ageing 20: 59, 2023.
48. Hagihara K, Haraguchi N, Nishimura J, Yasueda A, Fujino S, Ogino T, Takahashi H, Miyoshi N, Uemura M, Matsuda C *et al*: PLXND1/SEMA3E promotes epithelial-mesenchymal transition partly via the PI3k/AKT-signaling pathway and induces heterogenity in colorectal cancer. Ann Surg Oncol 29: 7435-7445, 2022.
49. Jurcak NR, Rucki AA, Muth S, Thompson E, Sharma R, Ding D, Zhu Q, Eshleman JR, Anders RA, Jaffeeet EM, *et al*: Axon guidance molecules promote perineural invasion and metastasis of orthotopic pancreatic tumors in mice. Gastroenterology 157: 838-850.e6, 2019.
50. Sun M, Chen Z, Song Y, Zhang B, Yang J and Tan H: PLXND1-mediated calcium dyshomeostasis impairs endocardial endothelial autophagy in atrial fibrillation. Front Physiol 13: 960480, 2022.
51. Mehta V, Pang KL, Rozbesky D, Nather K, Keen A, Lachowski D, Kong Y, Karia D, Ameismeier M, Huang J, *et al*: The guidance receptor plexin D1 is a mechanosensor in endothelial cells. Nature 578: 290-295, 2020.
52. Silva-Rodríguez P, Fernández-Díaz D, Bande M, Pardo M, Loidi L and Blanco-Teijeiro MJ: *GNAQ* and *GNA11* Genes: A Comprehensive review on oncogenesis, prognosis and therapeutic opportunities in uveal melanoma. Cancers (Basel) 14: 3066, 2022.
53. Gilman AG: G proteins: Transducers of receptor-generated signals. Annu Rev Biochem 56: 615-649, 1987.
54. Rodbell M: Nobel Lecture. Signal transduction: Evolution of an idea. Biosci Rep 15: 117-133, 1995.
55. Ha JH, Jayaraman M, Yan M, Dhanasekaran P, Isidoro C, Song YS and Dhanasekaran DN: *GNAi2/gip2*-regulated transcriptome and its therapeutic significance in ovarian cancer. Biomolecules 11: 1211, 2021.
56. Raymond JR Jr, Appleton KM, Pierce JY and Peterson YK: Suppression of GNAI2 message in ovarian cancer. J Ovarian Res 7: 6, 2014.
57. Lapitz A, Azkargorta M, Milkiewicz P, Olaizola P, Zhuravleva E, Grimsrud MM, Schramm C, Arbelaiz A, O'Rourke CJ, Casta AL, *et al*: Liquid biopsy-based protein biomarkers for risk prediction, early diagnosis, and prognostication of cholangiocarcinoma. J Hepatol 79: 93-108, 2023.
58. Polak ME, Borthwick NJ, Johnson P, Hungerford JL, Higgins B, Di Palma S, Jager, MJ and Cree IA: Presence and phenotype of dendritic cells in uveal melanoma. Br J Ophthalmol 91: 971-976, 2007.
59. de Waard-Siebinga I, Hilders CG, Hansen BE, van Delft JL and Jager MJ: HLA expression and tumor-infiltrating immune cells in uveal melanoma. Graefes Arch Clin Exp Ophthalmol 234: 34-42, 1996.
60. Wang W, Zhao H and Wang S: Identification of a novel immune-related gene signature for prognosis and the tumor microenvironment in patients with uveal melanoma combining single-cell and bulk sequencing data. Front Immunol 14: 1099071, 2023.
61. Seth R, Messersmith H, Kaur V, Kirkwood JM, Kudchadkar R, McQuade JL, Provenzano A, Swami U, Weber J, Alluri KC, *et al*: Systemic therapy for melanoma: ASCO Guideline. J Clin Oncol 38: 3947-3970, 2020.
62. Qi Y, Cui Q, Zhang W, Yao R, Xu D and Zhang F: Long non-coding RNA GAS5 targeting microRNA-21 to suppress the invasion and epithelial-mesenchymal transition of uveal melanoma. Cancer Manag Res 12: 12259-12267, 2020.
63. Tay Y, Rinn J and Pandolfi PP: The multilayered complexity of ceRNA crosstalk and competition. Nature 505: 344-352, 2014.
64. Barbagallo C, Di Maria A, Alecci A, Barbagallo D, Alaimo S, Colarossi L, Ferro A, Di Pietro C, Purrello M, Pulvirenti A and Ragusa M: VECTOR: An integrated correlation network database for the identification of CeRNA axes in uveal melanoma. Genes (Basel) 12: 1004, 2021.